

A Survey of Preprocessing and Feature Extraction Techniques for Radiographic Images

ERNEST L. HALL, MEMBER, IEEE, RICHARD P. KRUGER, MEMBER, IEEE, SAMUEL J. DWYER, III, MEMBER, IEEE, DAVID L. HALL, ROBERT W. MCLAREN, MEMBER, IEEE, AND GWILYM S. LODWICK

Abstract—Feature extraction is one of the more difficult steps in image pattern recognition. Some sources of difficulty are the presence of irrelevant information and the relativity of a feature set to a particular application. Several preprocessing techniques for enhancing selected features and removing irrelevant data are described and compared. The techniques include gray level distribution linearization, digital spatial filtering, contrast enhancement, and image subtraction. Also, several feature extraction techniques are illustrated. The techniques are divided into spatial and Fourier domain operations. The spatial domain operations of directional signatures and contour tracing are first described. Then, the Fourier domain techniques of frequency signatures and template matching are illustrated. Finally, a practical image pattern recognition problem is solved using some of the described techniques.

Index Terms—Feature extraction, pattern recognition, preprocessing, signatures, spatial filtering, template matching.

I. INTRODUCTION

THE need for computer-aided diagnosis in radiography is becoming increasingly urgent due to the expanding population and the continuing demand for improved quality medical care. For example, several million radiographs are read by radiologists each year. The use of computers in radiology can free the radiologist from routine tasks while providing more accurate measurements that may lead to more consistent diagnoses.

The design of a computer-aided diagnostic system may be divided into three phases: image pattern recognition, evaluation, and implementation. The image pattern recognition problem is usually considered to consist of three major steps: 1) preprocessing, 2) feature extraction, and 3) classification.

The most difficult step in image pattern recognition is still, as it was stated some 15 years ago by Selfridge [1], "the extraction of significant features from a background of irrelevant detail." This is particularly relevant with respect to

Manuscript received December 2, 1970; revised April 1, 1971. This work was supported by NIGMS, Federal Grant 17729-01. A preliminary version of this paper was presented at the IEEE Symposium on Feature Extraction and Selection in Pattern Recognition, Argonne, Ill., October 5-7, 1970. The images presented in this paper were computed at the Image Analysis Laboratory, University of Missouri, Columbia, Mo.

E. L. Hall, R. P. Kruger, S. J. Dwyer, III, and R. W. McLaren are with the Department of Electrical Engineering, University of Missouri, Columbia, Mo. 65201.

D. L. Hall and G. S. Lodwick are with the Department of Radiology, University of Missouri, Columbia, Mo. 65201.

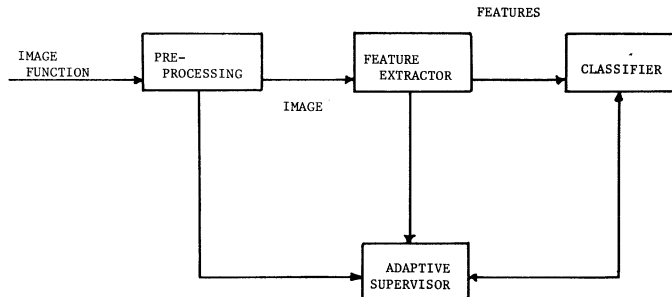


Fig. 1. Realistic pattern recognition system for image processing.

radiographic image analysis. Several authors, such as Uhr [2], have even cautioned against assuming the existence of significantly distinguishable features. An obvious example is that quite different three-dimensional objects can yield identical two-dimensional projections. The question about features has not raised serious doubts in biomedical image processing, mainly because feature extraction and pattern classification can be accomplished with reasonable success by radiologists. Thus, a more pertinent question might be the following. Can a computer successfully duplicate or compete with the procedures employed by a trained radiologist?

Practical models for the pattern recognition of images have been discussed by Levin [3], Tretiak [4], and others. The block diagram of a realistic pattern recognition system for image analysis is shown in Fig. 1. Image preprocessing usually consists of an application-dependent technique for enhancing preselected features or for removing irrelevant detail. The feature extractor will thus have an image function for its input. The purpose of this step is to extract features from the image. The features may contain coordinates, areas, average values, topological functions, etc., but must consist of a real-valued vector function of a set of images. The outputs of the feature extractor are then used by a pattern classifier. The following theoretical difficulty has been shown by Nagy [5]. The features must be evaluated in terms of the classification stage rather than during the feature extraction process. This results in the need for an adaptive supervisor. At the present time this adaptive supervisor is represented in most of our applications by a radiologist or a programmer.

Most image processing techniques which have been applied to biomedical situations have been found to be very application dependent. Thus, starting with a large repertoire of techniques, one can converge toward the best technique for a particular application. Previous applications of computer processing of radiographic images have been concerned with system compensations, improvement in resolution, image enhancement, and feature extraction for pattern recognition [6]–[8].

The purpose of this paper is to describe several preprocessing and feature extraction techniques which have been found to be useful for computer processing of radiographic images. The preprocessing techniques are designed to enhance selected features and eliminate irrelevant data. The feature extraction techniques are designed to extract specified, application-dependent information from a digitized radiographic image.

In Section II, the characteristics of radiographic images are briefly reviewed. Section III describes the preprocessing techniques, which include spatial digital filtering and image subtraction. Several examples are presented. Some feature extraction techniques are described in Section IV. These techniques are divided into spatial and Fourier domain methods. The spatial domain techniques consist of directional signatures and contour tracing. The Fourier domain techniques include frequency signatures and template matching. Finally, a simple but practical example of computer-aided diagnosis of rheumatic heart disease is presented.

II. RADIOGRAPHIC IMAGE CLASSIFICATION

The diagnostic information content in a radiograph is more semantic than statistical in nature. That is, the features necessary for diagnosing a particular disease are determined both by the disease and the class of images. For example, heart size is relevant in the diagnosis of rheumatic heart disease, but is probably irrelevant in the diagnosis of lung cancer. Also, the resolution required in a particular disease application may, for example, be an order of magnitude lower than that necessary for all general diseases using the same class of images.

A radiographic image is produced by permitting an X-ray source to penetrate an object and expose a photographic film. The intensity of exposure of a particular point on the film depends primarily on the object density and the source-object-film geometry. The X-ray tube has a finite focal spot which limits resolution. Also, phosphor intensifying screens are employed which hasten film exposure but decrease resolution.

The information content of a radiograph depends upon the absorption characteristics of the object, which are determined by the thickness, density, and material properties of the object exposed at a selected X-ray energy level. The resolution of a radiographic recording system depends primarily upon the X-ray focal spot size [9], the speed of the image intensifier screen(s) used [10], object scatter and motion, and the object-film distance. X-ray image contrast

is affected primarily by kilovoltage rating, and in a secondary way by object scatter. In addition, the random effect of quantum mottle, resulting from spatial changes in X-ray illumination, adds independent noise to the image.

Thus, radiographs are characterized by their low resolution and low contrast ratios of small features superimposed onto uniform backgrounds.

III. PREPROCESSING TECHNIQUES

In this section, several useful preprocessing techniques will be described. The techniques are designed to enhance the extraction of selected features and to eliminate irrelevant information in an image. First, a distribution linearization technique will be described. Second, spatial digital filtering methods using the fast Fourier transform or recursive partial difference equations will be described. Third, a contrast enhancement technique is illustrated. Finally, image subtraction, a simple technique for removing irrelevant information, is considered.

Distribution Linearization

Because image digitization requires that each gray level value be quantized over a finite range (e.g., six bits/picture element), a histogram of the gray level distribution values may be computed.

The gray level histogram (first-order probability density function) of most images exhibits a brightness peak which is heavily biased to the dark side of the histogram [8], [11], [12]. Fig. 2, a 64-level histogram of the chest radiograph shown in Fig. 3 is an example of this. The digital representation of the radiograph has 256×256 brightness values over a 33×33 cm face, with a sampling frequency in either dimension of 0.78 lines/mm. The effect of having a large percentage of the 65 536 picture elements (pixels) concentrated into such a narrow portion of the histogram is an image with little visible detail. Many contrast ratios that define edges are simply not displayable. One technique frequently used to correct this is the position-invariant nonlinear application of a software or hardware logarithmic conversion of the brightness pixels. This yields pixels which are proportional to image film density rather than brightness [13]. The log operation has the effect of expanding the gray range of the lower brightness pixels while compressing that of the higher brightness pixels. However, because of the shape of the brightness histogram, there is much more contrast expansion than compression. Fig. 4 is a gray level histogram of the original chest radiograph after logarithmic conversion.

Because a more rectangular histogram is advantageous, a position-invariant nonlinear-histogram equalization technique, similar to the distribution transform in statistics [14], is useful. Since the distribution transformation is only true for continuous variables, some care must be taken to obtain the desired result for the discrete approximation. If the histogram of Fig. 2 is summed from left to right, a monotone nondecreasing first-order distribution function is formed, as shown in curve 1 of Fig. 5. The ordinate of this curve is

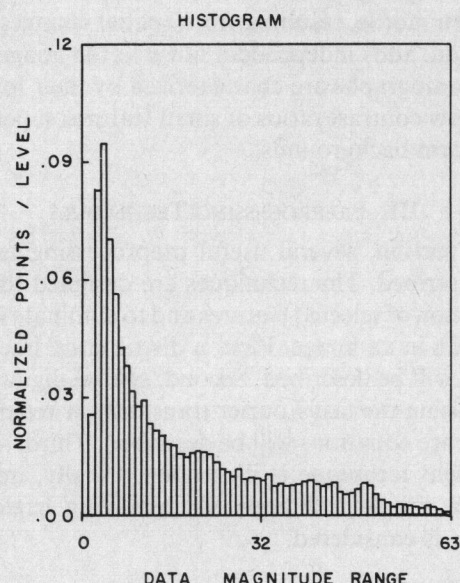


Fig. 2. Gray level histogram of original intensity image.

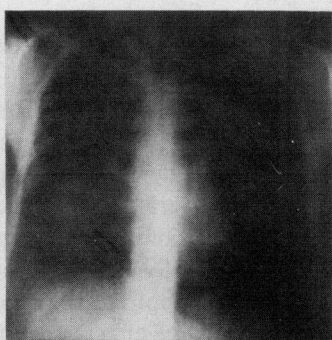


Fig. 3. Original chest radiograph.

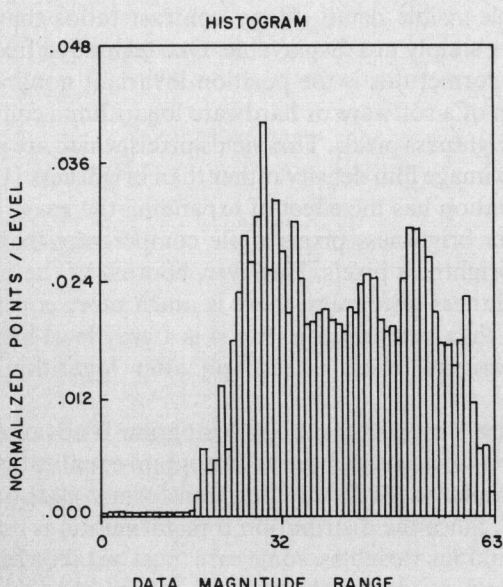


Fig. 4. Gray level histogram of density image.

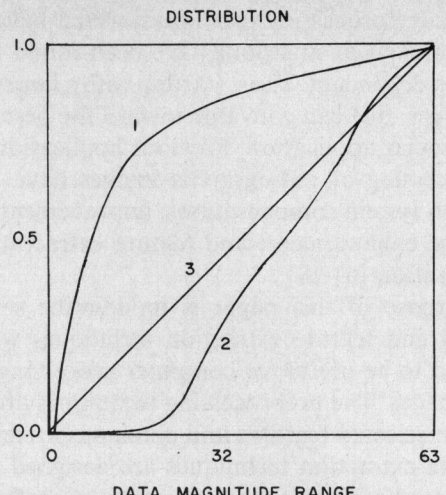


Fig. 5. Gray level distribution curves.

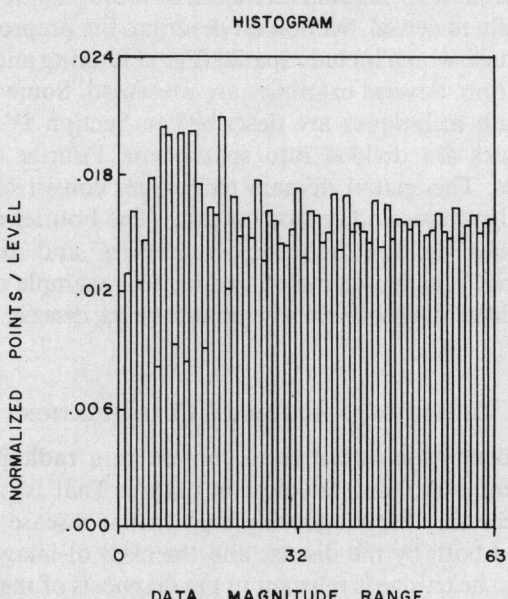


Fig. 6. Gray level histogram of linearized distribution image.

rescaled and divided into G equal increments with $G+1$ boundary points. The $G+1$ boundary points are then matched to their respective $G+1$ abscissa values. Each original image pixel is then *reassigned* to one of the new G levels corresponding to the appropriate abscissa increment. The resulting histogram, Fig. 6, is the best discrete approximation to a rectangular histogram. Its distribution function is shown in curve 3 of Fig. 5. Curve 2 of Fig. 5 is the distribution curve corresponding to the histogram of Fig. 4. Of the images tested, those using histogram equalization displayed more visible detail than those displayed after either software or hardware log conversion.

Linear Filtering

Several techniques for spatial and frequency domain design of spatial digital filters will now be considered.

The discrete Fourier transform for a square image function $p(m, n)$ is defined by

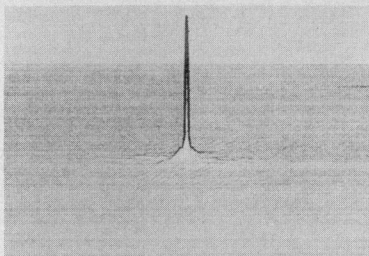


Fig. 7. Fourier transform magnitude.

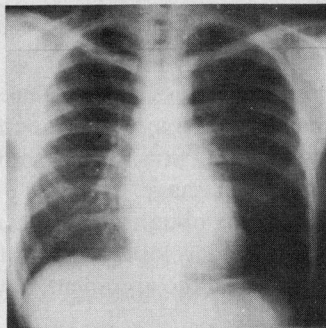


Fig. 8. Result of distribution linearization.

$$F[p] = \hat{P}(u, v) = \sum_{m=0}^{N-1} \sum_{n=0}^{N-1} p(m, n) e^{-2\pi j(um + vn)/N} \quad (1)$$

$$F^{-1}[\hat{P}] = p(m, n) = \frac{1}{N^2} \sum_{u=0}^{N-1} \sum_{v=0}^{N-1} \hat{P}(u, v) e^{2\pi j(um + vn)/N}. \quad (2)$$

Due to the sampled nature of p , the function \hat{P} and p are now both discrete, periodic in their respective variable pairs, and will be considered defined for all integers. The values of \hat{P} are the first N^2 terms of the Fourier series.

Another important property of the discrete Fourier transform is the symmetric conjugate property for real data, which necessitates storing only $N^2/2$ complex numbers in order to completely specify the transform of $p(m, n)$. Finally, origin centered arrays, convenient for transform space viewing and photography, can be obtained by multiplying each $p(m, n)$ by $(-1)^{m+n}$ prior to transformation [15].

Fig. 7 is the magnitude transform space of the image shown in Fig. 8. The center value (zero frequency coefficient) contains the image dc level (average image gray level). The higher energy, lower frequency components, radially surrounding the center, contain much of the image contrast information. The low-energy higher frequency coefficients are primarily responsible for image edge information. The transform of Fig. 7 is indicative of most two-dimensional Fourier transforms. The sampling frequency in this example is 0.78 l/mm over a square image. Thus the maximum frequency on both axes is 0.39 l/mm.

If $h(m, n)$ is the point spread function of a digital filter in two-space with a corresponding transfer function $\hat{H}(u, v)$, the filtered output image P_o can be arrived at by either

$$p_o(m, n) = F^{-1}[\hat{P}(u, v) \cdot \hat{H}(u, v)] \quad (3)$$

or

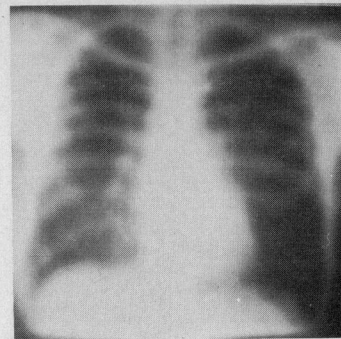


Fig. 9. Chest X-ray after low-pass filtering.

$$p_o(m, n) = \sum_{i=0}^{N-1} \sum_{k=0}^{N-1} p(i, k) h\{[m-i], [n-k]\} \quad (4)$$

where

$$\begin{aligned} [m-i] &= (m-i) \bmod N \\ [n-k] &= (n-k) \bmod N. \end{aligned}$$

In the two-dimensional case, if the point spread function h is real and circularly symmetric, then its transform is also real and circularly symmetric (isotropic). Under these conditions, the two-dimensional Fourier transform can be treated as a one-dimensional Hankel transform. Thus, for the case of isotropic filters, knowledge of h or \hat{H} profiles specifies the filter.

Isotropic filters are feasible primarily because of their design flexibility, and also because the magnitude transform space of many radiographs is not obtrusively nonisotropic.

When an image is low-pass filtered, the image contrast is generally unaffected. However, edge detail is effectively removed [16]. This effect is seen in the image displayed in Fig. 9. The most common application of low-pass filtering of images is to reduce the effect of random picture noise when the image is used for measurement selection and pattern recognition purposes. Other types of filters can be developed based on a low-pass prototype. A high-pass filter can be specified as

$$h_{HP}(m, n) = \delta_o - h_{LP}(m, n)$$

or

$$\hat{H}_{HP}(u, v) = 1 - \hat{H}_{LP}(u, v) \quad (5)$$

where

$$\delta_o = \begin{cases} 1, m, n = 0 \\ 0, \text{ elsewhere.} \end{cases} \quad (6)$$

The effect on an image as seen in Fig. 10 is to remove the contrast information of the image while outlining edges. The edge outlining effect can be seen most obviously at sharp high-contrast ratio edges, such as along the patient's diaphragm. A major application of high-pass filters is in the visualization of small low-contrast features superimposed onto uniform backgrounds [11], [12].

A filter which partially suppresses the lower frequency

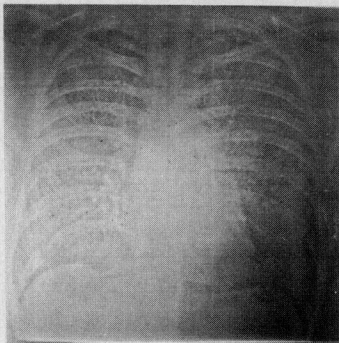


Fig. 10. Chest X-ray after high-pass filtering.

components while enhancing those higher is the high-emphasis filter. It can be formed from the high-pass filter as follows:

$$\begin{aligned}\hat{H}_{HE}(u, v) &= \alpha \hat{H}_{HP}(u, v) + 1 \\ h_{HE}(m, n) &= \alpha h_{HP}(m, n) + \delta_o, \alpha > 1.\end{aligned}\quad (7)$$

Clearly, as α becomes larger, the filter approaches the high-pass case. It should be noted that both the high-emphasis and high-pass filters create negative brightness pixels. These usually appear as dark bands surrounding the sharper high-contrast ratio edges in an image. The application of a high-emphasis filter to an image has an effect on image edges quite similar to the photographic technique of unmasked sharpening [13]. This technique overemphasizes edges, reinforcing the Mach phenomenon. The filtering result is shown in Fig. 11.

Another method for performing linear spatial digital filtering is by partial difference equations. The motivation for using partial difference equations for filtering is the possible reduced computation and memory storage requirements. It is sometimes possible to obtain an order of magnitude speed advantage with small memory requirements. The disadvantages of this method are that the design techniques are not as versatile as the FFT and filter stability problems must be considered.

Design techniques for obtaining a desired response have been developed [17], [18]. These techniques require the use of the two-dimensional z -transform, defined in (8) for a picture function, $p(m, n)$,

$$ZW\{p(m, n)\} = \sum_{n=0}^{\infty} \sum_{m=0}^{\infty} p(m, n) z^{-m} w^{-n} \quad (8)$$

where the region of convergence is of the form $|z| > R_{cz}$; $|w| > R_{cw}$. The ZW -transform is useful because it leads to a systematic method for solving partial difference equations. Two of the most important properties of the transform are the shifting property and the convolution property [18]. The convolution property allows one to determine a filter transfer function. The frequency response of the system may be determined by simply replacing z by $e^{j\omega_x \Delta x}$ and w by $e^{j\omega_y \Delta y}$ in the filter transfer function, where ω_x and ω_y denote the spatial frequencies, and Δx and Δy denote the sampling intervals in the x and y directions, respectively. The frequency response is generally complex, so that both magni-

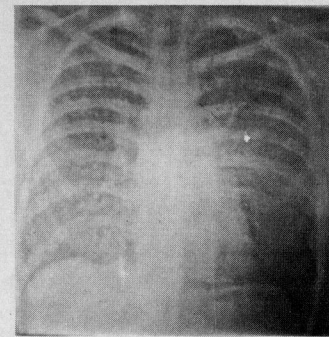


Fig. 11. Chest X-ray after high-frequency emphasis filtering via FFT.

tude and phase response must be considered. A nonlinear phase response can produce a large amount of ringing in the filter point spread function, which shows up as large dark bands in the filtered image.

A design technique to obtain a desired magnitude frequency response can be developed by noting that squared trigonometric functions of the argument, θ , where

$$\theta = \frac{\omega_x \Delta x}{2}, \quad \theta = \frac{\omega_y \Delta y}{2}$$

or

$$\theta = \frac{\omega_x \Delta x + \omega_y \Delta y}{2} \quad (9)$$

corresponds to rational functions of z and w or of the product, $q = zw$. Thus, a design procedure similar to the one-dimensional technique of Gold and Rader [19] can be used.

A four-pole Butterworth spatial digital filter was designed by this method. The filter was realized by the parallel combination of 2 two-pole filters. Each two-pole filter was implemented with a partial difference equation of the form shown in (10).

$$\begin{aligned}p_o(m, n) &= (1 + \alpha) p(m, n) - 2\alpha p_o(m - 1, n - 1) \\ &\quad - \alpha p_o(m - 1, n - 2) + b p_o(m - 2, n - 1) \\ &\quad + c p_o(m - 2, n - 2)\end{aligned}\quad (10)$$

where α is the high-emphasis factor, and b and c are related to the poles of the filter.

The result of filtering the image shown in Fig. 3 with the high-emphasis filter is shown in Fig. 12.

Postfiltering Contrast Enhancement

While high-emphasis filtering is useful as an edge sharpening procedure, it has the somewhat undesirable effect of reducing image contrast. Fig. 13 shows the gray level distribution curves of the example radiograph for a high-pass filter, curve 1, and three high-emphasis filters with $\alpha = 1, 2, 3$, curves 2, 3, and 4, respectively, with the filters being identical in other respects. A procedure that has been quite useful for increasing image contrast is the nonlinear position invariant mapping, shown in Fig. 14. This procedure maps a filtered image p_o on the abscissa onto a contrast-enhanced image p_{oc} on the ordinate. The threshold values were set by

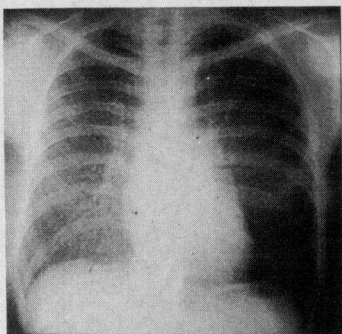


Fig. 12. Chest X-ray after high-frequency emphasis filtering via recursive filter.

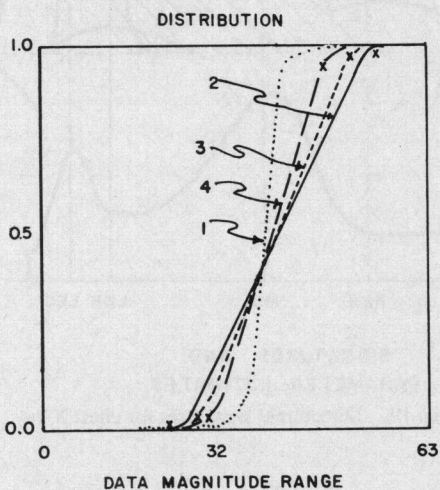


Fig. 13. Gray level distribution curves of filtered images.

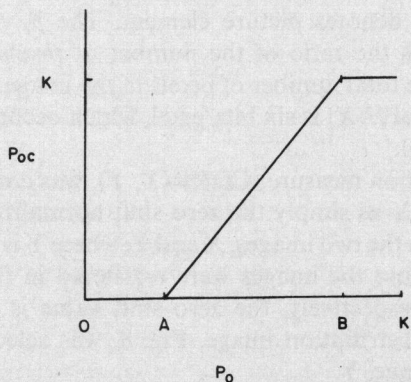


Fig. 14. Contrast enhancement mapping.

counting the S negative pixels formed by high-emphasis filtering. Negative pixels are often encountered in digital spatial filtering and are displayed by simply scaling the image before displaying. In each case, the thresholds were located on the knee or elbow of the distribution curve, indicating that comparably few pixels are involved. The darkest pixels mapped into zero are primarily those corresponding to the negative overshoot of highest contrast ratio most acute edges. Those mapped into K are primarily the corresponding positive overshoot. A similar gray level transformation may be developed with the distribution linearization technique, which has the added advantage of

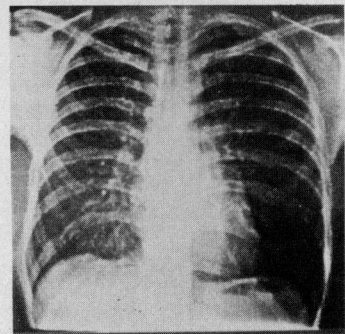


Fig. 15. Chest X-ray after high-frequency emphasis filtering and contrast enhancement.

being adaptive. Fig. 15 is an example of contrast enhancement by distribution linearization of the high-emphasis filtered image shown in Fig. 11. This technique visually enhances the image because the edge sharpness is retained while contrast ratios that define small edges are expanded.

Image Subtraction

When two radiographs differ only in certain details, a subtraction of the two images can be performed to accentuate the differences in the two films.

Image subtraction is a commonly used technique in serial angiography [20]. In serial angiography, a radio-opaque substance is injected into an artery. The blood passing the needle during injection becomes radio-opaque and thus is visible on a radiograph as it passes through the various phases of the circulation. The photographic subtraction method requires precise registration of the films, a precise inverse relation between the copy print negative and the original, correct exposure, and controlled development of gamma 1.0.

The subtraction may also be performed digitally. Although prevention of motion, correct exposure, and precise registration are still important, a contact print is not necessary. The effects of motion, exposure, and registrations can also be compensated for on the computer. Registration must be carefully accomplished during scanning and small adjustments may be made by correlation or matched filtering.

An example of the digital image subtraction is shown in Figs. 16–18. The original image consists of a hand X-ray, X , and an arteriogram, A . The images were subtracted point-by-point with the following simple algorithm.

$$RA = \begin{cases} A - X & \text{if } A - X > 0 \\ 0 & \text{if } A - X \leq 0 \end{cases}$$

RA : resulting artery image. (11)

The resulting image value was set to zero if the difference was negative because this information could only correspond to bone or tissue residues and not to arterial information. The resulting image is also shown in Fig. 18. Image subtraction could be a very useful preprocessing step for extracting arterial or venous features with contour following machine algorithms. The original hand X-ray indicates a normal bone and tissue structure. The arteriogram, however, shows an abnormal arterial structure be-



Fig. 16. Original hand X-ray.



Fig. 17. Hand arteriogram showing arterio-venous abnormality.

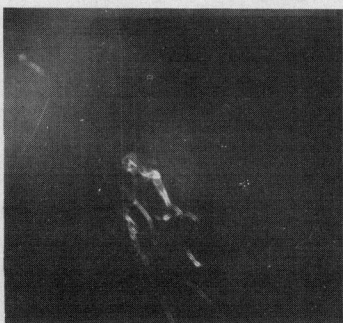


Fig. 18. Subtraction result.

tween the first and second fingers. The subtracted image shows the overall arterio-venous malformation and much of the detail structure which was previously not visible.

Evaluation

The most effective method of comparing images at present is subjective human evaluation. However, some calculable quantitative measure for comparing preprocessing results is desired. Three such quantities have been computed for the images, as indicated in Figs. 9-12 and 15. These are: 1) a first-order entropy measure; 2) a zero-shift correlation value; and 3) the combined mean and mean-square error.

A first-order entropy measure [21] was computed from a 64-gray level histogram of each image. The 64-gray level calculation is compatible with the number of gray levels of the output display. The computation is given by

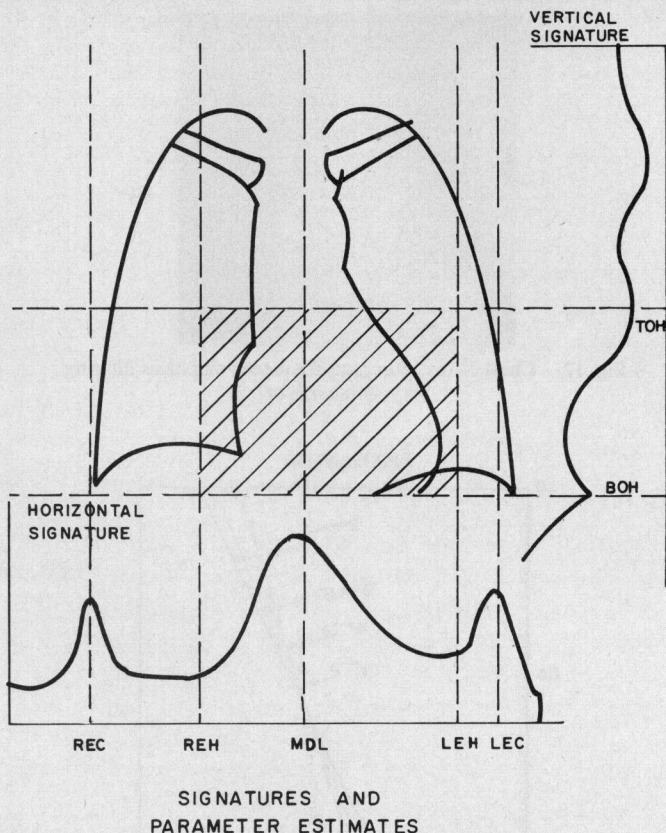


Fig. 19. Directional signatures for chest X-ray.

$$H(X) = - \sum_{i=0}^{63} p_i \log_2 p_i \text{ bits/pixel} \quad (12)$$

where pixel denotes picture element. The p_i values were computed as the ratio of the number of pixels with gray level i , to the total number of pixels in the image. The maximum value of $H(X)$ is six bits/pixel, which occurs when the p_i 's are equal.

A correlation measure, $\text{CORR}(X, Y)$, was computed for each image X as simply the zero shift normalized correlation between the two images, X and Y , where Y is a reference image. Because the images were registered in the x and y directions, respectively, the zero shift value is maximum. The linear distribution image, Fig. 8, was selected as the reference image, Y .

Mean error and mean-square error were also computed between each processed image X and the reference image Y , Fig. 19. A difference image, $Z = X - Y$, was first computed. The mean u and variance σ^2 over all picture elements of Z are directly related to the mean-square error (MSE) as given by

$$\text{MSE} = N^2(u^2 + \sigma^2) \quad (13)$$

where N^2 is the total number of pixels. To effect a comparison, it is easier to use the error mean and variance, because these values are normalized to accommodate the number of pixels. The error values are in units/pixels, the mean error ranges over 0 to 63.

TABLE I
CALCULATED MEASURES

Measure Image	Entropy $H(X)$ Bits/Pixel	Correlation CORR (X, Y)	Mean $-\mu -$ Units/Pixel	Error Calculation Variance $-\sigma^2 -$ (Units/Pixel) 2
Linear Distribution (Reference- Y) Fig. 8	5.981	1.000	0.000	0.000
Low-Pass Filtered Fig. 9	5.938	0.997	0.088	8.356
High-Pass Filtered Fig. 10	2.963	0.873	4.065	322.714
High-Emphasis FFT Fig. 11	3.988	0.918	1.836	223.331
High-Emphasis REC Fig. 12	5.007	0.985	9.999	101.981
High-Emphasis FFT with Contrast Enhancement Fig. 15	5.982	0.936	-0.095	174.602
Original Scaled Fig. 3	5.276	0.948	16.185	57.194

The experimental calculations of the three measures are presented in Table I. Note that the entropy measure is much lower for the high-pass and high-emphasis filtered images than for the low-pass or original image. The correlation measure is largest for the recursive high-emphasis and low-pass filtered images. The mean error is noticeably larger for the original image, because all of the filtered images were computed from the reference image.

IV. FEATURE EXTRACTION

As previously defined, feature extraction consists of the extraction of significant features from a background of irrelevant detail. Methods for the enhancement of selected features and elimination of irrelevant detail were described in Section III. In this section, several techniques for the extraction of significant features from an image function will be described.

The selection of an image feature set is a significant problem in itself, and no general theoretical solution exists. One reason for this difficulty is that the set of features required for classification of normal or abnormal samples for a particular disease is relative not only to the class of images but also to the diagnostic problem under consideration. Also, information which is pertinent to one diagnostic problem may be irrelevant to the solution of another problem. Note that the general problem of normal or abnormal classification, with respect to general health, is not being considered. Obviously, this problem requires more information for a successful solution than is available on any set of radiographs. Therefore, a practical approach to selecting a feature set has been used by the authors. That is, the initial set of features for a given application is selected as the set used by radiologists. With these limitations in mind, several techniques for the extraction of significant features will now be described.

The feature extraction techniques considered here may be divided into spatial domain or Fourier domain operations, although most techniques may be considered in either domain. Two useful spatial domain techniques, directional

signatures and contour tracing algorithms, will be described first. Then, two Fourier domain methods, frequency signatures and template matching, will be described. Finally, a simple classification example will be described.

Directional Signatures

A simple but powerful technique for locating objects in fixed frame images consists of gray level directional signatures, e.g., Meyers *et al.* [22]. A fixed frame image set consists of images of similar objects; for example, chest, head, or leg X-rays. Normalization is a significant but solvable problem. The directional signature consists of a function which is the sum of the gray level pixel values along a line normal to a reference line. The x and y direction signatures for a chest X-ray are shown in Fig. 19. Note that major objects such as the clavical, the lungs, the heart, and the diaphragm may be located from the signatures. The signature information allows one to "zoom" in on a particular object. After an object has been located, measurements such as size or texture may be made.

Contour Tracing

A study of the human visual system (HVS) gives important insights into the feature extraction problem. It is known that the HVS responds linearly to the logarithm of the observed image brightness. It is also known that the subjective effect of image acuity or sharpness is more closely related to the rendition of objects much larger than those barely visible [10], [23]. The Mach phenomena relates to the physiological fact that the eye creates dark and light bands near contours of abrupt changes in image brightness and that this phenomena results in the subjective enhancement of a sharp brightness change. In summary, the HVS is most sensitive to contrast ratios and acuity properties of image edges, and least sensitive to the absolute brightness levels.

This knowledge of the importance of edge structure to the HVS has been used to advantage by Graham [24] and others to develop data compression techniques. A radiologist in

diagnosing a patient's condition from a radiograph, also obtains a large amount of information from visible line or boundary structure.

These facts clearly indicate the importance of edge structure as significant features in many radiographic images, and motivate the development of computer algorithms for extracting edge information.

A common intuitive notion of an edge is as a border between objects of different intensities in an image. Since many functions satisfy this transition criteria, an edge detector must be relatively insensitive to variations in the shape of this edge function. The ideal edge detector would also be insensitive to amplitude, position, and rotation. If all edges have the same shape, and if variations from the edges can be characterized as additive noise, then the optimum edge detector is a matched filter. A useful approximation to the optimum filter can be developed by assuming no noise and developing a filter template which is a space reversed replica of the ideal edge.

The correlation of an edge function and detector is shown in Fig. 20. From this it is clear that larger values of α will result in larger peak values of the correlation; however, the width of the response also increases so that resolution is decreased. Furthermore, the output due to noise points will decrease with increasing α .

A two-dimensional edge detector which is approximately rotationally invariant and simple to implement is developed as follows. Two one-dimensional detectors, one orientated horizontally and one vertically, are used. The absolute values of the two outputs are added to produce the correlation output. The ratio of edge intensity to background intensity is quite large. Thus, this output is well suited for use with a contour tracing algorithm.

Several algorithms have been developed for tracing contours in images [6], [24]. These algorithms start by considering the image as a relief map with brightness representing elevation. Boundary regions are then represented by long narrow ridges. Noise points show up as sharp mountains. One could use the lines of equal elevation to describe the contours. However, a more sensitive algorithm results from attempting to follow the ridges. The algorithm used is a refinement of the method used by Graham [24] and Campbell [6]. An example is shown in Fig. 21.

Fourier Transform Frequency Signatures

The utility of spatial frequency power-spectrum sampling for automatically classifying patterns in images was demonstrated by Lendaris and Stanley [25], with particular applications to detecting targets in aerial photographs. The purpose of this section is to consider the applications to biomedical images.

The usefulness of frequency sampling is based on the fact that certain features of an image function may be more distinguishable in the frequency domain than in the spatial domain. A large data reduction may also be effected and the features still distinguished.

The frequency signature consists of a set of n samples, where n is the number of sampling areas for a given sam-

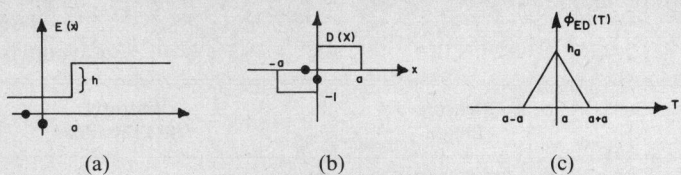


Fig. 20. Correlation of an edge function with edge detector. (a) One-dimensional edge detection, idealized edge. (b) One-dimensional edge detection, correlation detector. (c) One-dimensional edge detection, correlation of detector with edge function.

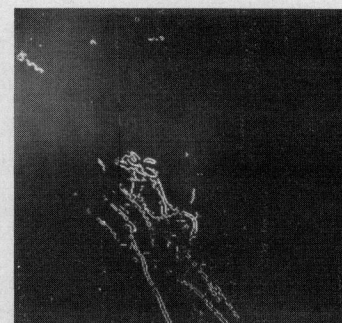


Fig. 21. Ridge followed contour trace of hand subtraction result.

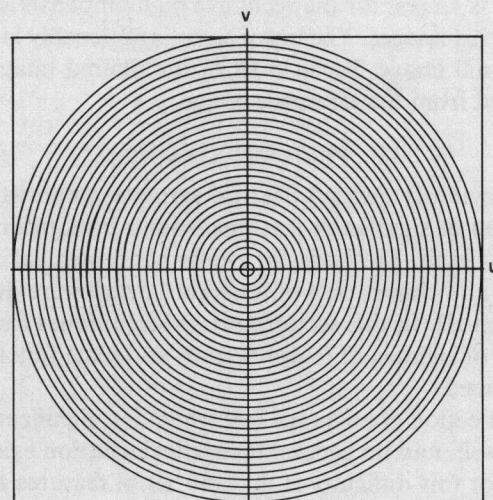


Fig. 22. Annular ring sampling geometry.

pling geometry. Several sampling geometries may be used. An annular ring sampling geometry, Fig. 22, is suited to the detection of circular objects. A wedge-shaped geometry can be used to detect periodic line structures in an image. A horizontal or vertical slit may be used to detect on axis features. An example of this technique will now be presented. A well-known property of the two-dimensional Fourier transform is that the transform of a circularly symmetric object is also circularly symmetric. Thus, if one is trying to detect circular objects an annular ring sampling geometry is appropriate. Peaks in this circular sampled signature would correspond to energy at a given radial distance in the transform space.

A class of images which is suitable to this analysis is electron microscope images of cells. One particular problem is the detection of mitochondria. Mitochondria are generally circular or oval structures which are surrounded by a double

walled membrane about 180 Å thick. Inside the fluid filled bodies are minute rod-like objects about 3 to 4 μm in length. The inner wall of the body folds in to form a complex structure. The presence of other structures such as nuclei, endoplasmic reticulum, golgi apparatus, red blood corpuscles, normal variations due to age and type subject, angle of preparation slice, etc., make feature extraction algorithms difficult to implement. Gray level histograms may be used to distinguish certain cells [26]; however, this method does not detect more complex bodies, such as mitochondria. Our preliminary results indicate that a circular frequency sample will distinguish between mitochondria and other structures. Several images and their corresponding circular signatures are shown in Figs. 23–26. The location and amplitude of peaks in the signatures may be used as input features for a decision rule.

Template Matching

Suppose that an image function of known form, $s(x, y)$, which is nonzero only over a finite rectangular region ($0 \leq x \leq X$, $0 \leq y \leq Y$), is perturbed by additive noise. The filter which maximizes the ratio of signal power to average noise power at the filter output at some spatial position ($\Delta x, \Delta y$) is called a matched filter. A detection decision may be made by sampling the matched filter output at the position ($\Delta x, \Delta y$) and comparing this value to a threshold.

If $S^*(u, v)$ is the conjugate of the Fourier transform of the signal and $|N(u, v)|^2$ is the power spectrum of the noise, then the matched filter transfer function $H(u, v)$ is given by

$$H(u, v) = \frac{S^*(u, v)}{|N(u, v)|^2} e^{-j(\omega_x \Delta x + \omega_y \Delta y)}. \quad (14)$$

The occurrence of the noise power spectrum factor in the equations for $H(u, v)$ can be interpreted as a prewhitener for colored noise.

This form of the matched filter has been developed for the simple detection of a signal whose location is known. Instead of searching over all filter outputs, one need only sample at ($\Delta x, \Delta y$) to obtain the best detection results. Since the location of the signal is usually not known, the correlation implementation of the optimum filter is more useful in image pattern recognition.

Suppose that the noise is white, i.e., $|N(\omega)|^2 = 1$ and that the input to the filter is $g(x, y)$ and $s(x, y)$. One form of Schwarz's inequality may be used to show that the normalized cross correlation can take on the value 1 only at displacements at which $g(x, y)$ is matched to $s(x, y)$ to a multiplicative constant. Therefore, the position of objects may be determined by locating the peaks in the matched filter output. The delay ($\Delta x, \Delta y$) shifts the peak a known amount.

A matched filter detection is not affected by a translation of the signal; however, it is sensitive to rotation. Andrews [27] discusses an interesting way to remove rotation sensitivity. The matched filter is also sensitive to magnification changes. If only a small size variation in the desired signal is expected, then a search through several sizes may be reasonable.



Fig. 23. Frequency signature image, endoplasmic reticulum.

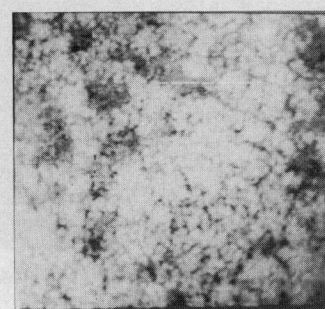


Fig. 24. Frequency signature image, glycogen.

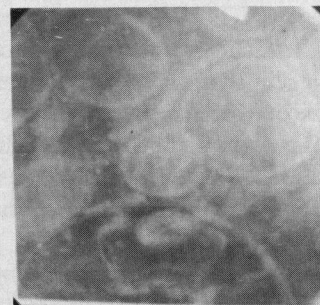


Fig. 25. Frequency signature composite image: mitochondria, glycogen, and endoplasmic reticulum.

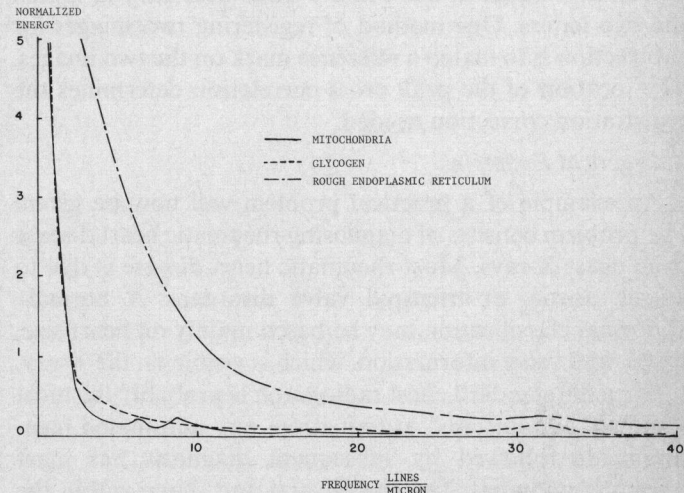


Fig. 26. Frequency signatures of example images.

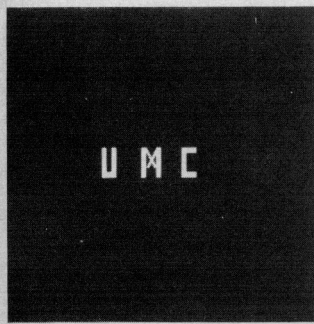


Fig. 27. Characters UMC.

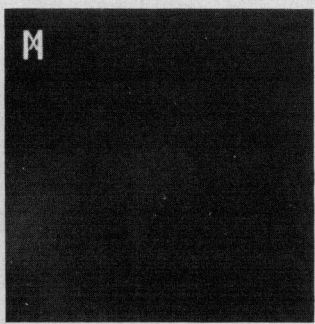


Fig. 28. Template character.

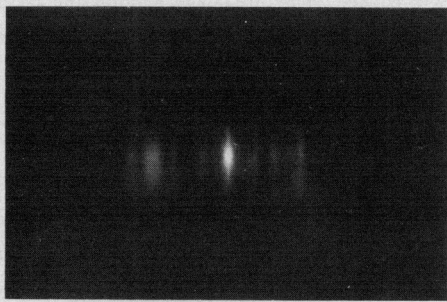


Fig. 29. Result of template matching.

The digital matched filter output may be computed by spatial convolution or by use of the two-dimensional fast Fourier transform (FFT). The tradeoff between the two methods is well known [6]. If the number of nonzero template points is less than 132, then convolution is faster. Another difference between the two methods is that the FFT method computes a periodic convolution while spatial convolution is aperiodic. This sometimes causes a detection peak to "wraparound" from one side of the image to the other.

An example of binary template matching for letters is shown in Figs. 27–29. The letter M is the template and is easily detected from the letters UMC by thresholding the correlation of the two images. The position of the threshold detection is equal to the x and y shifts necessary to match the two letters. One method of registering two images for subtraction is to match a reference mark on the two images. The location of the peak cross correlation determines the registration correction needed.

A Practical Example

An example of a practical problem will now be given. The problem consists of diagnosing rheumatic heart disease from chest X-rays. Most rheumatic heart disease is due to mitral, aortic, or tricuspid valve disorders. A normal-abnormal classification may be based mainly on heart size, shape, and valve information, which is visible on the X-ray.

Since the standard chest radiograph is probably the most routinely administered examination, any automated measurements followed by subsequent diagnosis has mass screening potential. The cardiac size and shape within the pleural cavity is often used in diagnosis. Automated measurement of cardiac size and shape descriptors has been undertaken by Kruger [20] to obtain normal-abnormal and

differential diagnoses for a group of acquired valvular lesions resulting from rheumatic fever as well as a normal-abnormal classification for a mixed group of other abnormalities. In this problem, the significant features to be extracted are the right and left heart and vascular boundaries and the area and extent measurements associated with them.

The first task was to reliably detect the anatomical location of the heart within the pleural cavity. This was accomplished using the horizontal and vertical spatial signatures shown in Fig. 19. The chest midline (MDL) was computed as the maximum intensity value on the horizontal signature. The right and left cardiac extent (REH and LEH) were estimated using the method of parabolic smoothed first derivatives. The right and left chest boundary (REC and LEC) were taken to be the largest intensity values before REH and after LEH, respectively. The top of heart (TOH) and bottom of heart (BOH) were likewise estimated using the smoothed derivative approach. The estimated TOH and BOH values were then used to compute a second horizontal signature and all measures but MDL were estimated again. Finally the iterated value of LEH and MDL were used to create a second vertical signature from which TOH was reestimated. The preceding procedure inscribed an approximate heart area within a cardiac rectangle of dimensions (BOH-TOH) by (LEH-REH). Since the heart is of greater intensity than the area around it within this rectangle, the smoothed first derivative inflection point of the integrated gray level histogram was used to create a binary representation within the rectangle. The right and left cardiac-vascular borders were easily found by detecting two successive zeros either way from the midline. Termination of the contours at the right and left cardiac-diaphragm intercepts were then accomplished using smoothed first- and second-order derivatives. Two examples of a detected contour are shown in Figs. 30 and 31. These examples indicate the extremes of the detection problem. Fig. 32 shows the above measurements. It should be noted that line measurements were normalized with respect to Thr and all area measurements were normalized with respect to a rectangular area PA which is an approximation to the pleural cavity. These parameters as well as coefficients of least squares fourth-order polynomial approximations to both vascular-cardiac boundaries (LP and RP) were given to the classification algorithm which initially determined an abnormal or normal diagnosis. Further subdivision into four abnormal classes for the rheumatic cases has also been accomplished. The differential diagnosis is structured in the five following classes: 1) normals; 2) mitral valvular stenosis only; 3) mitral valvular stenosis and insufficiency; 4) both valves involved with stenosis and/or insufficiencies; 5) aortic valvular involvement only with stenosis and/or insufficiency. A discriminant function $d_{ij}(\bar{x})$ is computed for each pair of classes (say i and j). The n -vector \bar{x} is the output of the feature extraction algorithm. For this pair, a sample \bar{x} is "rejected" twice from class i or j depending on $d(\bar{x})$ being positive or negative, and \bar{x} is "rejected" once from each class (i and j) if $d=0$. \bar{x} is classified (after all pairs of classes

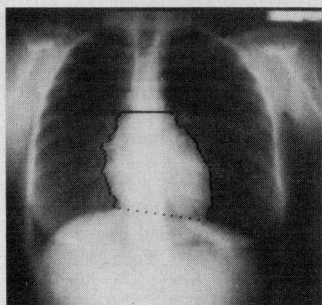


Fig. 30. Small normal heart outlined.

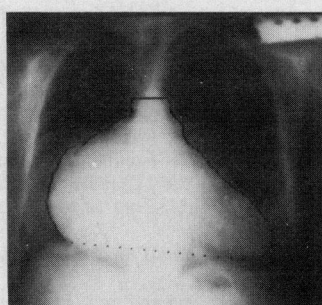


Fig. 31. Extremely large heart outlined.

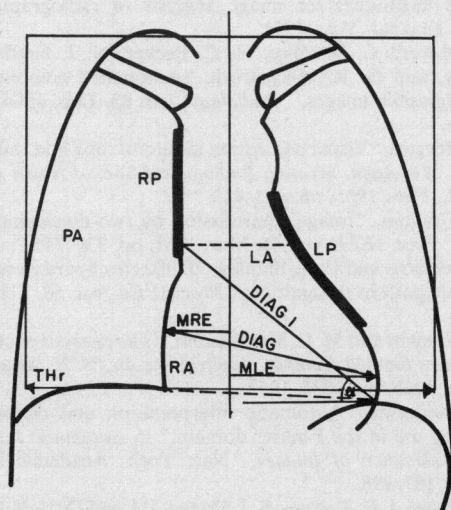


Fig. 32. Anatomical features measured. Thr: thoracic distance; MLE: maximum left cardiac extent; MRE: maximum right cardiac extent; CTR: cardiothoracic ratio ($Ml + Mr$)/Thr; LA: cardiac area left of midline; RA: cardiac area right of midline; DIAG: diagonal cardiosthacic ratio; DIAG1: diagonal distance from right cardiac apex to left cardiac-diaphragm intercept; α : angular measurement of DIAG1 from horizontal; LP: left polynomial; RP: right polynomial; TA: RA + LA; PA: as shown.

have been considered) into the class with the minimum number of "rejections." For example, suppose we have the following. Then x would be said to be in class 1.

	Class	Number of "Rejections"
$d_{12}(x) < 0$	1	2
$d_{13}(x) < 0$	2	5
$d_{14}(x) < 0$	3	4
$d_{15}(x) > 0$	4	5
$d_{23}(x) < 0$	5	4
$d_{45}(x) < 0$		

TABLE II-A
CLASSIFICATION RESULTS—TRAINING

	Computer Choice				
	1	2	3	4	5
Cardiac	1	84	1	3	1
Catheterization	2	1	26	5	2
Result	3	2	1	48	1
	4	0	2	0	19
	5	0	0	1	1
					53

Normal versus Abnormal Percent Correct	97 Percent
Percent of True Normals Which Were Called Normal	95 Percent
Percent of True Abnormals Which Were Called Abnormal	98 Percent

Percent Diagnosed Correctly for Each Class	
Class	Rate (Percent)
1	95
2	77
3	87
4	83
5	97

Average percent correct overall classes	90
---	----

TABLE II-B
CLASSIFICATION RESULTS—TEST

	Computer Choice				
	1	2	3	4	5
Cardiac	1	80	3	3	0
Catheterization	2	3	18	9	0
Result	3	4	3	43	0
	4	1	2	11	5
	5	6	1	12	1
					37

Normal Versus Abnormal Percent Correct	91 Percent
Percent Normals Called Normal	90 Percent
Percent Abnormals Called Abnormal	92 Percent

Percent Diagnosed Correctly for Each Class	
Class	Rate (Percent)
1	90
2	57
3	76
4	22
5	65

Average percent correct overall classes	73
---	----

For this study $d(\bar{x})$ was chosen to have one of two possible forms: 1) linear function in \bar{x} , 2) a quadratic function in \bar{x} .

Thus if $\bar{x} = (x_1, \dots, x_n)$, $d(\bar{x})$ is one of

$$d(\bar{x}) = a_0 + a_1 x_1 + \dots + a_n x_n$$

or

$$d(\bar{x}) = a_0 + a_1 x_1 + a_{11} x_1^2 + a_2 x_2 + a_{12} x_1 x_2 + a_{22} x_2^2 + \dots$$

for some appropriate set of a 's.

The normal-abnormal diagnoses were similarly structured. The classification results for a training sample and a test sample are given in Table II for the rheumatic heart study only. The testing results were obtained by removing ten percent of the data from each class and training on the

remaining 90 percent. The removed ten percent was then tested. This procedure was repeated until all data had been removed and tested. Table II shows the results obtained from 264 films.

V. SUMMARY

In this paper, preprocessing techniques for enhancing selected features and removing irrelevant detail have been described. The techniques consisted of gray level, distribution linearization, spatial digital filtering, contrast enhancement, and image subtraction. Several examples were given and three evaluation measures were computed for seven of the processed images. Next, some useful feature extraction techniques were described. The techniques were divided into spatial domain and Fourier domain operations. The spatial domain technique of directional signatures often allows one to "zoom in" on an object of interest. The importance of edge information and contour tracing were also emphasized. The Fourier domain technique of frequency signature sampling was also demonstrated. Next, matched filtering for detection of well-defined objects was illustrated. Finally, a practical feature extraction and classification example using some of the previous techniques was described.

The techniques required for a practical problem are very dependent on the application. However, starting with a large repertoire of techniques allows one to quickly select the proper ones for a given application.

REFERENCES

- [1] O. G. Selfridge, "Pattern recognition and modern computers," in *Proc. Western Joint Comput. Conf.*, Mar. 1955, pp. 91-93.
- [2] L. Uhr, "Feature discovery and pattern recognition," in *Pattern Recognition*, L. N. Kanal, Ed. Washington, D.C.: Thompson, 1969, pp. 159-181.
- [3] M. D. Levine, "Feature extraction: A survey," *Proc. IEEE*, vol. 57, Aug. 1969, pp. 1391-1407.
- [4] O. J. Tretiak, "Pattern recognition," Mass. Inst. Technol., Cambridge, Mass., Notes of Image Proc. Workshop, June 1970.
- [5] G. Nagy, "State of the art in pattern recognition," *Proc. IEEE*, vol. 56, May 1968, pp. 836-862.
- [6] J. D. Campbell, "Edge structure and the representation of pictures," Ph.D. dissertation, Dep. Elec. Eng., Univ. of Missouri, Columbia, Aug. 1969.
- [7] "Image processing, basic techniques and applications," Mass. Inst. Technol., Cambridge, Mass., M.I.T. Summer Workshop Notes, July 1968.
- [8] A. V. Oppenheim, R. W. Schafer, and T. G. Stockham, "Nonlinear filtering of multiplied and convolved signals," *Proc. IEEE*, vol. 56, Aug. 1968, pp. 1264-1291.
- [9] D. Kunio, "Optical transfer function of the focal spot of X-ray tubes," *Amer. J. Rad. Ther. Nucl. Med.*, Oct. 1965.
- [10] R. H. Morgan, "An analysis of the physical factors controlling the diagnostic quality of roentgen images," *Amer. J. Rad. Ther. Nucl. Med.*, Dec. 1965.
- [11] R. P. Kruger and S. J. Dwyer, "Image analysis of radiographs," SWIEECO Tech. Papers, Dallas, Tex., Apr. 1970, pp. 147-149.
- [12] R. Selzer, "Improving biomedical image quality with computers," Jet Propulsion Lab., Calif. Inst. Tech., Pasadena, Calif., Tech. Rep. 32-1336, Oct. 1968.
- [13] C. R. Neblette, *Photography, Its Materials and Processes*. Princeton, N. J.: Van Nostrand, 1951.
- [14] R. V. Hogg and A. T. Craig, *Introduction to Mathematical Statistics*. New York: Macmillan, 1965.
- [15] H. C. Andrews, "Fourier coding of images," Ph.D. dissertation, Univ. of Southern California, June 1968.
- [16] A. Rozenfeld, *Picture Processing by Computer*. New York: Academic Press, Inc., 1969.
- [17] J. S. Shanks, "Two-dimensional recursive filters," SWIEECO Rec. Tech. Papers, Dallas, Tex., Apr. 1969.
- [18] E. L. Hall and S. J. Dwyer, III, "Frequency domain design of spatial digital filters," presented at the IEEE Inform. Theory Conf., June 1970; also Image Analysis Lab., Univ. of Missouri, Columbia, Tech. Rep. 101, June 1970, p. 121.
- [19] B. Gold and C. M. Rader, *Digital Processing of Signals*. New York: McGraw-Hill, 1969.
- [20] W. H. Oldendorf, "Subtraction and auto-subtraction techniques for reproducing radiographs," *J. Biol. Photogr. Ass.*, vol. 32, May 1964, pp. 65-76.
- [21] R. P. Kruger, E. L. Hall, S. J. Dwyer, III, and G. S. Lodwick, "Digital techniques for image analysis of radiographs," *Int. J. Biomed. Comput.*, Apr. 1971.
- [22] P. H. Meyers, C. M. Nice, H. C. Becker, N. J. Nettleton, J. W. Sweeney, and G. R. Meckstroth, "Automated computer analysis of radiographic images," *Radiology*, vol. 83, Dec. 1964, pp. 1029-1034.
- [23] R. H. Morgan, "Visual perception in fluoroscopy and radiography," in *Proc. 51st Annu. Meeting Radiological Soc. of North Amer.*, Chicago, Ill., Nov. 1965, pp. 403-416.
- [24] D. N. Graham, "Image transmission by two-dimensional contour coding," *Proc. IEEE*, vol. 55, Mar. 1967, pp. 336-346.
- [25] G. G. Lendaris and G. L. Stanley, "Diffraction-pattern sampling for automatic pattern recognition," *Proc. IEEE*, vol. 58, Feb. 1970, pp. 198-216.
- [26] J. M. S. Prewitt and M. L. Mendelsohn, "The analysis of cell images," in *Advances Biomed. Comput. Applications An.* (N. Y. Acad. Sci.), vol. 128, Jan. 1966, pp. 1035-1053.
- [27] H. C. Andrews, "Automatic interpretation and classification of images by use of the Fourier domain," in *Automatic Interpretation and Classification of Images*. New York: Academic Press, Inc., 1969, pp. 187-198.
- [28] R. P. Kruger, J. R. Townes, S. J. Dwyer, III, and D. Hall, "Computer aided diagnosis via feature extraction and classification of radiographic cardiac size and shape descriptors," presented at the 9th Annu. Symp. Biomath. and Comput. Sci in Life Sci., Houston, Tex., Mar. 1971, 22-24.